IEEE Access
Multidisciplinary | Rapid Review | Open Access Journal

Received August 30, 2018, accepted October 8, 2018, date of publication October 17, 2018, date of current version November 14, 2018.

Digital Object Identifier 10.1109/ACCESS.2018.2876393

Optimization Model Based Sub-Nyquist Sampling of Pulses With Various Shapes and Its Application to ECG Signals

GUOXING HUANG, NING FU, (Member, IEEE), AND LIYAN QIAO, (Member, IEEE)
Department of Automatic Test and Control, Harbin Institute of Technology, Harbin 150080, China
Corresponding author: Ning Fu (funinghit@163.com)

This work was supported by the National Natural Science Foundation of China under Grant 61671177 and Grant 61102148.

ABSTRACT Recently developed variable pulse width finite rate of innovation (VPW-FRI) theory offers an efficient way for sampling pulse streams with various shapes at the sub-Nyquist rate. Unfortunately, for real signals, noise, and model mismatch will induce inaccuracies to such scheme in the reconstruction process. In this paper, an optimization model-based sub-Nyquist sampling system for pulses with various shapes is proposed, which improves the performance of VPW-FRI scheme under noise and model mismatch situation. Since the real pulse streams with various shapes may be modeled as the sum of an unknown number of Lorentzian pulses and a model mismatch error signal, we build an optimization object function with the purpose of minimizing the energy of this model mismatch error signal. Then, for solving such function, we propose a two-channel sub-Nyquist sampling system to obtain a Fourier coefficients subset and several discrete samples from the input signal. We demonstrate that the best number of Lorentzian pulses and the corresponding pulse parameters can be found by using an improved particle swarm optimization algorithm. Finally, simulations with the electrocardiogram signals in MIT-BIH database have shown that the proposed method has better performance and stability than traditional VPW-FRI scheme.

INDEX TERMS Optimization, sub-Nyquist, finite rate of innovation (FRI), electrocardiogram (ECG), model mismatch, pulse streams.

I. INTRODUCTION

Signals consisting of the sum of a few pulses are widely used in wireless communication [1]–[3], biomedicine [4], [5] and radar [6]–[8]. Such signals can be determined uniquely with the amplitude parameters and time delay parameters of the pulses. According to the Nyquist sampling theorem [9], to perfectly recover a signal from the samples, the sampling rate should satisfy the Nyquist rate, i.e., twice the maximum frequency of the signal. However, for wide-band pulses, such theorem becomes challenging since it is very hard to build hardware operating at very high rate. Recently, the finite rate of innovation (FRI) scheme [10]–[12] has been proposed as a sub-Nyquist sampling scheme for streams of pulses with known shapes. It was shown that, perfect parameter estimation is allowed by uniformly sampling the filtered version of the FRI signals at a much lower rate, nearly equal to the rate of innovation, i.e., the average number of degrees of freedom per unit of time.

Various FRI sampling kernels have been proposed, among which are Sinc kernel and Gaussian kernel in [10], B-spline, E-spline and rational kernels in [13], SoS (Sum of Sincs) kernel in [14]. In addition to streams of Diracs, these kernels give the FRI theory more flexibility to retrieve short pulses with more generic shapes. However, these kernels are hard or impossible for hardware realization. To reduce the complexity of the system's hardware design and improve the noise resistance, several muti-channel FRI sampling systems are proposed. Gedalyahu *et al.* [15] proposed a multi-channel FRI sampling system based on mixers and integrators, in which the discrete Fourier coefficients can be obtained. Unfortunately, since only one Fourier coefficient can be obtained in a single channel, such system has a complex structure characterized by a large number of sampling channels. To obtain several Fourier coefficients subsets distributed over the signal spectrum, Baransky *et al.* [16] proposed another multi-channel sampling scheme. However, to avoid spectrum aliasing, such system obtained the Fourier coefficients subsets by using a redundant and complex approach. So in [17] we have presented a simplified FRI sampling scheme with similar functions. To further solve the spectrum aliasing

problem, we proposed another system in [18] to obtain the real part of the signal spectrum.

Note that, for all above FRI sampling systems, the input pulse streams are required to have the same pulse shape, which is fixed and needs to be known apriori. However, in many applications, such as the electrocardiogram (ECG), the pulse shapes are various throughout the signal. There are many pulse functions, such as the B-spline and E-spline functions, the Gaussian functions, the wavelet basis functions and the Lorentzian functions, can be used for approximating the pulses with various shapes. Based on these functions, several extended FRI schemes have been proposed. Maravic *et al.* [19] approximated the Fourier coefficients of each pulse with polynomials and proposed a low-sampling rate channel estimation for digital ultrawideband (UWB) receivers. However, in order to approximate the pulse shapes better, a large polynomial degree is required, which means a high sampling rate. Zhang and Dragotti [20], [21] developed an extended FRI sampling theory for signals consisting of pulses with unknown shapes. However, it requires that each pulse can be represented as a sparse signal in the wavelet domain, which is not common in practice. Nagesh and Seelamantula [22] proposed an asymmetric model based on the sum of a Guassian pulse and its fractional Hilbert transform, aiming to model part of ECG signals and characterizing ventricular hypertrophy. However, due to the fixed pulse width, such scheme may not converge to a satisfactory result. In [23]–[25], the authors introduced the Lorentzian functions in modeling the pulses with various shapes and then developed the Variable Pulse Width FRI (VPW-FRI) sampling theory. Since there are four free parameters, namely the symmetry and asymmetric amplitudes, the time delay and the pulse width, in each Lorentzian function, it allows some stability and flexibility in modeling the pulses with various shapes. Unfortunately, such technology turns to be unstable under noise and model mismatch situations.

In this paper, we consider the problem of sub-Nyquist sampling of pulse streams with various shapes under noise and model mismatch situations. Based on the VPW-FRI framework in [23]–[25], we model the practical pulse streams as the sum of an unknown number of Lorentzian pulses and a model mismatch error signal. In order to find the best number of Lorentzian pulses and other pulse parameters, we propose a two-channel sub-Nyquist sampling system. One channel obtains a Fourier Coefficients subset from the signal spectrum, which is used to initially estimate the unknown parameters of the Lorentzian pulses. The samples of the other channel are used to optimize these parameters by minimizing the energy of the model mismatch error signal. Finally, simulation results of the real electrocardiogram (ECG) pulses demonstrate that the proposed system outperforms the VPW-FRI scheme under noise and model mismatch situations.

The rest content of this paper is arranged as follows: The problem formulation is given in Section II and a brief review of VPW-FRI is introduced in Section III. Our sampling system is proposed in Section IV. The recovery algorithm and some practical considerations of real ECG signals are proposed in Section V. We analyze the performance our system and compare it with some related works using some simulations in Section VI. Finally, a brief conclusion is given in Section VII.

II. PROBLEM FORMULATION

In this paper, the problem of sub-Nyquist sampling of pulse streams with various shapes is considered. As shown in [23]–[25], the Lorentzian pulses bring more versatility and flexibility in modeling such signals. Considering the noise and model mismatch situations, we model such signals with the sum of an unknown number of Lorentzian pulses and a model mismatch error signal, that is,

$$x(t) = \sum_{k=1}^{K} f_k(t) + \sigma(t),\ 0 \le t < \tau, \tag{1}$$

where τ is the time duration of the signal $x(t)$ and K is the number of Lorentzian pulses. The functions $f_k(t)$, with $k = 1, 2, \cdots, K$, are the Lorentzian pulses which can be divided into

$$f_k(t) = f_k^s(t) + f_k^a(t), \tag{2}$$

where

$$f_k^s(t) = c_k \frac{r_k}{\pi\left(r_k^2 + (t - t_k)^2\right)}, \quad r_k > 0,\ t_k \in [0, \tau), \tag{3}$$

and

$$f_k^a(t) = d_k \frac{t - t_k}{\pi\left(r_k^2 + (t - t_k)^2\right)}, \quad r_k > 0,\ t_k \in [0, \tau). \tag{4}$$

Here, $f_k^s(t)$ and $f_k^a(t)$ are symmetric and anti-symmetric parts of the Lorentzian pulse $f_k(t)$, respectively. Obviously, each Lorentzian pulse $f_k(t)$ can be determined uniquely by 4 parameters: symmetric amplitude c_k, anti-symmetric amplitude d_k, pulse width r_k and time delay t_k. Such function offers more versatility and flexibility than the simpler symmetric functions, which are only defined by amplitude and time delay parameters of the pulse. Since it is not common that a real signal completely matches the sum of Lorentzian pulses, we introduce the mismatch error signal $\sigma(t)$ in our model.

An example of a real ECG signal with an appropriate expression of our model is shown in Figure 1. The sum of 8 different Lorentzian pulses $\sum_{k=1}^{8} f_k(t)$ is represented in Figure 1(b) and the model mismatch error signal $\sigma(t)$ is depicted in Figure 1(c). We can see that this model offers an exactly equivalent expression of the ECG signal $x(t)$.

If the input signal $x(t)$ perfectly matches the VPW-FRI model in [23]–[25], that is, the number of Lorentzian pulses K is known and the model mismatch error $\sigma(t) = 0$. Then there are only $4K$ unknown parameters in (1), i.e., $\{c_k, d_k, r_k, t_k\}_{k=1}^{K}$. As shown in [23], these $4K$ unknown parameters can be estimated uniquely from only $2K + 1$

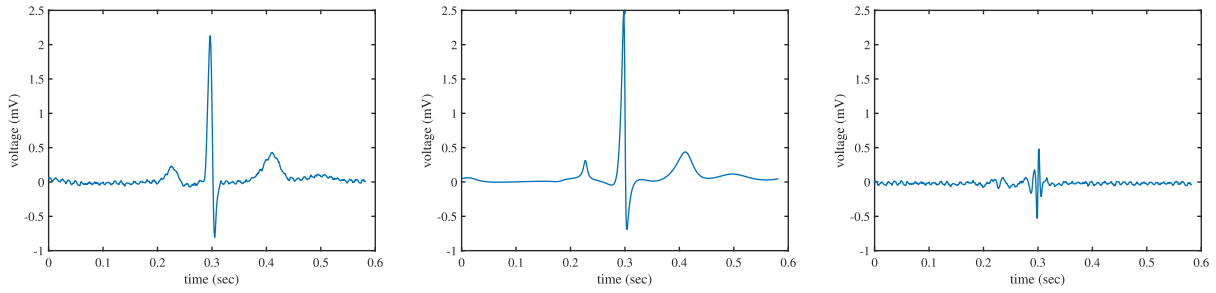

FIGURE 1. ECG signal model: (a) Real ECG signal $x(t)$; (b) Sum of 8 different Lorentzian pulses $\sum_{k=1}^{8} f_k(t)$; (c) Model mismatch error signal $\sigma(t)$.

continuous Fourier coefficients of the signal $x(t)$, described as

$$X[m] = \sum_{k=1}^{K} \frac{c_k - id_k}{\tau} e^{-2\pi m(r_k+it_k)/\tau} = \sum_{k=1}^{K} v_k u_k^m, \quad m \in \mathbb{Z}, \tag{5}$$

where $v_k = \frac{c_k - id_k}{\tau}$ and $u_k = e^{-2\pi m(r_k+it_k)/\tau}$. Note that the Fourier coefficients $X[m]$ have been restricted to positive indices ($m \geq 0$) for the convenience of calculation, as suggested in [23]. The problem in (5) is very often encountered in spectral estimation, and the parameters $\{v_k, u_k\}_{k=1}^{K}$ can be estimated uniquely by using the annihilating filter method in [10] or other spectral estimation methods in [26]–[30]. After that, we can estimate the pulse parameters as: $c_k = real(v_k\tau)$, $d_k = -imag(v_k\tau)$, $r_k = \frac{\tau \log|u_k|}{2\pi}$ and $t_k = -\frac{\tau \angle u_k}{2\pi}$. Here, $real(\cdot)$ is the real part of $(\cdot)$, $imag(\cdot)$ is the imaginary part of $(\cdot)$, $\log(\cdot)$ is the natural logarithm of $(\cdot)$ and $\angle(\cdot) \in [0, 2\pi)$ is the principle argument of $(\cdot)$.

However, the input signal usually does not perfectly match the VPW-FRI model, that is, the number of Lorentzian pulses K is usually unknown and the model mismatch error $\sigma(t) \neq 0$. This situation is very common since the pulse shapes of the signal are usually unknown in practice, and the sampling process may also introduce some noise. In this case, the traditional VPW-FRI technology needs to select an appropriate value for the number of Lorentzian pulses K with experience, which may lead to a large error of the reconstruction results. Moreover, as shown in [23]–[25], such model mismatch problem will lead the solution of (5) unstable. That is, some of the solutions $u_k = e^{-2\pi m(r_k+it_k)/\tau}$ are mapped outside a unit circle, corresponding to the fact that the estimated pulse width $r_k < 0$. In this paper, our goal is to propose a sub-Nyquist sampling method for signals with the model in (1), where the number of Lorentzian pulses K is unknown and the model mismatch error $\sigma(t) \neq 0$.

III. REVIEW OF VPW-FRI

In this section, we give a brief review of the VPW-FRI theory proposed in [23]–[25]. Formally, VPW-FRI framework

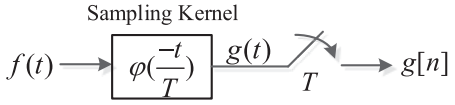

FIGURE 2. Sampling structure of VPW-FRI. Here, $f(t)$ is sum of Lorentzian pulses; $\varphi(t)$ is the sampling kernel; T is the sampling interval and $g[n]$ is the discrete-time samples.

considers the signals formed by the sum of some Lorentzian pulses. Such signals can be described as

$$f(t) = \sum_{k=1}^{K} \left[f_k^s(t) + f_k^a(t)\right], \quad 0 \leq t < \tau, \tag{6}$$

where the number of Lorentzian pulses K is known, $f_k^s(t)$ and $f_k^a(t)$ are given by (3) and (4) respectively. Obviously, we have $f(t) = x(t)$, only when the model mismatch error signal $\sigma(t) = 0$.

The VPW-FRI sampling structure is illustrated in Figure 2. Firstly, the signal $f(t)$ is filtered with the sampling kernel $\varphi(t)$, which is an ideal low-pass filter (LPF). After that, the filtered signal is sampled uniformly at the rate twice the cut-off frequency of the LPF. Then a set of Fourier coefficients $F[m]$ can be obtained by calculating the discrete Fourier transform (DFT) of the samples. Formally, the Fourier coefficients of $f(t)$ are

$$F[m] = \sum_{k=1}^{K} \left\{F_k^s[m] + F_k^a[m]\right\}, \tag{7}$$

where

$$F_k^s[m] = \frac{c_k}{\tau} e^{-2\pi(r_k|m|+jt_k m)/\tau}, \quad m \in \mathbb{Z}, \tag{8}$$

and

$$F_k^a[m] = -\frac{d_k}{\tau} sgn(m) e^{-2\pi(r_k|m|+jt_k m)/\tau}, \quad m \in \mathbb{Z}. \tag{9}$$

The absolute value $|m|$ derives from the conjugate symmetry of the spectrum. $F_k^s[m]$ and $F_k^a[m]$ are the Fourier coefficients of $f_k^s(t)$ and $f_k^a(t)$, respectively. Obviously, $F_k^s[m]$ is essentially the Hilbert transform of $F_k^a[m]$.

To estimate the unknown parameters of the Lorentzian pulses, i.e., $\{c_k, d_k, r_k, t_k\}_{k=1}^{K}$, from the obtained Fourier

coefficients $F[m]$, the annihilating filter method in [10] is used. Let $u_k = e^{-2\pi m(r_k+it_k)/\tau}$ and the filter

$$A(z) = \prod_{k=1}^{K}(1-u_k z^{-1}) = \sum_{l=1}^{K} A[l]z^{-l}, \tag{10}$$

then

$$\begin{aligned}(A*F)[m] &= \sum_{l=0}^{K} A[l]F[m-l] \\ &= \sum_{l=0}^{K}\sum_{k=1}^{K}(c_k - jd_k)A[l]u_k^{m-l} \\ &= \sum_{k=1}^{K}(c_k - jd_k)\underbrace{\left(\sum_{l=0}^{K} A[l]u_k^{-l}\right)}_{A(u_k)}u_k^m = 0, \end{aligned} \tag{11}$$

where the integer m is restricted to positive indices, i.e., $m \geq 0$, for the sake of calculation. Solving the filter coefficients $A[l]$ by (11) requires at least $2K+1$ non-negative Fourier coefficients $F[m]$. Then the parameters t_k and r_k can be estimated from the roots of filter $A(z)$, and other parameters c_k and d_k are retrieved by solving (11). Although the annihilating filter method works stable in the traditional FRI, it is not guaranteed in the VPW-FRI framework. As shown in [23], the unstable solutions correspond to the roots of the filter $A(z)$, i.e., $u_k = e^{-2\pi m(r_k+it_k)/\tau}$, mapped outside a unit circle. That is, the estimated Lorentzian pulse width $r_k < 0$. Such unstable solutions appear much more frequently under noise and model mismatch situations.

IV. OPTIMIZATION MODEL BASED VPW-FRI SAMPLING SYSTEM

In this section, we present a two-channel sub-Nyquist sampling system for signals with the model in (1), where the number of Lorentzian pulses K is unknown and the model mismatch error $\sigma(t) \neq 0$. The system structure is described in Section IV-A. In order to find the best number of Lorentzian pulses K and other unknown parameters $\{c_k, d_k, r_k, t_k\}_{k=1}^{K}$ of the input signal $x(t)$ in (1) with the samples from our system, we build an optimization object function with the purpose of minimizing the energy of the model mismatch error signal $\sigma(t)$, as shown in Section IV-B. Finally, the choice of the system parameters is analyzed in Section IV-C.

A. SYSTEM DESCRIPTION

In order to obtain a Fourier coefficients subset of the continuous-time signal $x(t)$ in (1), we use a low-pass filter (LPF) and an analog-to-digital converter (ADC) with the sampling rate twice the cut-off frequency of the LPF. In this way, a band of Fourier coefficients can be obtained by calculating the DFT of the samples. Besides the Fourier coefficients, we use an additional channel consisting of a simple low-rate ADC to obtain several time domain samples $x[n']$. Such additional sampling channel is designed to optimizing the recovery results of the main sampling channel.

The proposed sampling structure is illustrated in Figure 3. This system has two parallel sampling channels, with one consists of a LPF and an ADC in sequence, and the other only consists of a low-rate ADC.

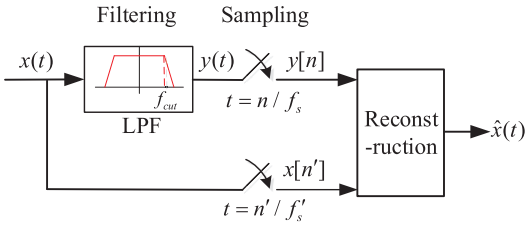

FIGURE 3. Block diagram of our system. The components include a LPF and two ADCs.

In the first sampling channel, the input signal $x(t)$ is filtered with a LPF. Assume that the impulse response of the LPF is $h(t)$ and the cut-off frequency of the LPF is f_{cut}. So the filtered signal is $y(t) = x(t) * h(t)$. After the filtering process, the filtered signal $y(t)$ is uniformly sampled at a rate $f_s \geq 2f_{cut}$ and the samples are

$$y[n] = x(t) * h(t)|_{t=n/f_s}, \quad 0 \leq n < N-1, \ n \in Z, \tag{12}$$

where $N = \lfloor \tau f_s \rfloor + 1$ is the number of samples.

Then we show how to obtain the Fourier coefficients of the input signal $x(t)$ from the samples $y[n]$ $(n = 0, 1, \cdots, N-1)$ in (12). Based on the DFT of $y[n]$, the Fourier coefficients of the filtered signal $y(t)$ can be calculated as

$$Y[m] = \frac{1}{f_s}\sum_{n=0}^{N-1} y[n]e^{-j\frac{2\pi}{N}mn}, \quad m = 0, 1 \cdots N-1. \tag{13}$$

Suppose that the signal spectrum is truncated by an ideal LPF with cut-off frequency f_{cut}, then we have

$$\begin{aligned} Y(f) &= rect(\frac{f}{2f_{cut}})X(f) \\ &= \begin{cases} X(f), & |f| \leq f_{cut} \\ 0, & |f| > f_{cut}, \end{cases} \end{aligned} \tag{14}$$

where $X(f)$ is the Continuous-Time Fourier Transform (CTFT) of the input signal $x(t)$. If we substitute $f = mf_0$, where m is an integer and $f_0 = 1/\tau$, (14) can be rewritten as:

$$Y[m] = X[m], \quad 0 \leq m \leq M-1, \tag{15}$$

where $M = \lfloor f_{cut}/f_0 \rfloor + 1$. The mathematical symbol $\lfloor(\cdot)\rfloor$ rounds the elements of $(\cdot)$ to the nearest integer less than or equal to that element. Note that the Fourier coefficients $X[m]$ have been restricted to positive indices $(m \geq 0)$ for the convenience of calculation, as mentioned in Section II. Thus, we can obtain $M = \lfloor \tau f_{cut} \rfloor + 1$ Fourier coefficients $X[m]$ $(m = 0, 1, \cdots, M-1)$ from the obtained samples $y[n]$ $(n = 0, 1, \cdots, N-1)$.

In the other parallel sampling channel, the input signal $x(t)$ is uniformly sampled at a rate $f_s' = 1/T_s'$ and the samples are

$$x[n'] = x(t)|_{t=n'/f'_s}, \quad 0 \leq n' < N'-1, \ n' \in Z, \tag{16}$$

where $N' = \lfloor \tau f_s' \rfloor + 1$ is the number of samples.

It is natural to wonder how to solve the aliasing of the sub-Nyquist samples. As illustrated in Figure 3, the proposed system consists of two parallel sampling channels. The first channel is used to obtain a few discrete frequency domain samples (i.e., Fourier coefficients) of the input signal. In this channel, a LPF is used to prevent frequency aliasing. According to the well known Nyquist sampling theorem [9], frequency aliasing can be avoided when the sampling rate of the ADC is twice the cut-off frequency of the LPF. Aliasing effect is nullified at a certain set of discrete frequencies by employing a suitable LPF, and the following time-domain samples thus obtained could be used to find the Fourier coefficients of the input signal at those discrete frequencies. The second channel is used to obtain several discrete time domain samples of the input signal. In the proposed system, only a few discrete frequency domain samples from the first channel and several discrete time domain samples from the second channel are required to reconstruct the input signal. Thus, if the system parameters are appropriate selected, aliasing wouldn't be a problem to our system.

B. OPTIMIZATION OBJECT FUNCTION

Before explaining the sampling scheme, we build an optimization model for approximating the input signal $x(t)$ with the sum of K Lorentzian pulses. In practice, we aim to find the most optimal number of Lorentzian pulses K and other unknown Lorentzian pulse parameters $\{c_k, d_k, r_k, t_k\}_{k=1}^K$ by minimizing the energy of the model mismatch error signal $\sigma(t)$ in (1). Such optimization problem can be described as

$$\min \int_0^\tau \sigma^2(t)dt. \tag{17}$$

Since $\sigma(t) = x(t) - \sum_{k=1}^K f_k(t)$, (17) may be rewritten as

$$\min \int_0^\tau \left(x(t) - \sum_{k=1}^K f_k(t) \right)^2 dt. \tag{18}$$

However, the optimization problem (18) can not be solved since the input signal $x(t)$ is unknown. So we replace $x(t)$ with its discrete samples $x[n']$ ($n' = 0, 1, \cdots, \lfloor \tau f_s' \rfloor$) given by (16). Then the optimization problem (18) is converted into

$$\min \sum_{n'=0}^{N'-1} \left(x[n'] - \sum_{k=1}^K f_k[n'] \right)^2, \tag{19}$$

where $\sum_{k=1}^K f_k[n'] = \sum_{k=1}^K f_k(t)|_{t=n'T_s'}$.

From (2) it can be seen that the sum of Lorentzian pulses $\sum_{k=1}^K f_k(t)$ can be determined uniquely by $4K$ parameters $\{c_k, d_k, r_k, t_k\}_{k=1}^K$. If the sampling rate $f_s' = 1/T_s'$ is known, then the sum of discrete Lorentzian pulses $\sum_{k=1}^K f_k[n']$ can also be determined by $4K$ parameters $\{c_k, d_k, r_k, t_k\}_{k=1}^K$. The optimization problem in (19) may be described as

$$\min fitness(K, \{c_k, d_k, r_k, t_k\}_{k=1}^K), \tag{20}$$

where

$$fitness(K, \{c_k, d_k, r_k, t_k\}_{k=1}^K) = \sum_{n'=0}^{N'-1} \left(x[n'] - \sum_{k=1}^K f_k[n'] \right)^2 \tag{21}$$

is called as the optimization object function. Our goal is to find the most optimal K and the corresponding $\{c_k, d_k, r_k, t_k\}_{k=1}^K$ with minimum $fitness(\cdot)$.

C. CHOICE OF PARAMETERS

An essential property of a FRI sampling system is that the sampling sequences provide enough Fourier coefficients to recover the unknown parameters, since otherwise recovery is impossible. For the signals perfectly match the VPW-FRI model in [23]–[25], we have determined in Section II that the unknown parameters $\{c_k, d_k, r_k, t_k\}_{k=1}^K$ can be estimated uniquely when the number of Fourier coefficients is more than $2K + 1$. Since we can obtain $M = \lfloor \tau f_{cut} \rfloor + 1$ Fourier coefficients $X[m]$ ($m = 0, 1, \cdots, M - 1$) from the obtained samples $y[n]$ ($n = 0, 1, \cdots, N - 1$) by (15), we recommend choosing the cutoff frequency of LPF as

$$\begin{aligned} \lfloor \tau f_{cut} \rfloor + 1 &\geq 2K + 1 \\ &\Rightarrow f_{cut} \geq 2K/\tau. \end{aligned} \tag{22}$$

The next uniformly sampling process should satisfy the Nyquist sampling theory to prevent aliasing. So the sampling rate of the first channel should satisfy

$$f_s \geq 2f_{cut} \geq 4K/\tau. \tag{23}$$

Note that the lowest sampling rate is $4K/\tau$ and it is far below the Nyquist rate of $x(t)$ in most cases.

However, in this paper, our interest focus on the more common signals which do not perfectly match the VPW-FRI model, that is, the model mismatch error signal $\sigma(t) \neq 0$ and the number of Lorentzian pulses K is unknown. In this case, the solution of (5) is usually unstable, as shown in [23]–[25]. The unstable solution corresponds to the fact that the estimated Lorentzian pulse width $r_k < 0$. So the misestimated parameters $\{c_k, d_k, r_k, t_k\}_{k\in\Psi}$ can be obtained from all estimated parameters $\{c_k, d_k, r_k, t_k\}_{k=1}^K$ by judging the value of each r_k. Here, $\Psi \subset \{1, 2, \cdots, K\}$ is the index set of the estimated Lorentzian pulses with negative width. According to (22), we have

$$K \leq \lfloor \tau f_{cut}/2 \rfloor. \tag{24}$$

So our system allows a unique recovering of at most $\lfloor \tau f_{cut}/2 \rfloor$ pulses. The range of choices of the number of Lorentzian pulses K is $\{1, 2, \cdots, \lfloor \tau f_{cut}/2 \rfloor\}$.

We use another sampling channel to find the optimal number of Lorentzian pulses K, as well as to find the optimal solutions to replace the unstable solutions. For each selected $K \in \{1, 2, \cdots, \lfloor \tau f_{cut}/2 \rfloor\}$, the parameters $\{c_k, d_k, r_k, t_k\}_{k=1}^K$ can be estimated from the obtained Fourier coefficients by using the spectral estimation methods in [26]–[29]. Then we

can easily calculate the sum of Lorentzian pulses $\sum_{k=1}^{K} f_k(t)$ by (2) and calculate its discrete version as $\sum_{k=1}^{K} f_k[n'] = \sum_{k=1}^{K} f_k(t)|_{t=n'/f'_s}$. In order to solve optimization problem of (20), at least $N' \geq 1$ time domain samples $x[n']$ ($n' = 0, 1, \cdots, N'-1$) is required. So the sampling rate of the additional channel must satisfies

$$\begin{aligned} N' &= \lfloor \tau f'_s \rfloor + 1 \geq 1 \\ &\Rightarrow f'_s \geq 1/\tau. \end{aligned} \tag{25}$$

Note that such sampling rate f'_s should be properly increased to reduce the effect of noise. In fact, we set $f'_s = f_s$ for convenience. Finally, the optimization problem of (20) can be solved, for example, by using the particle swarm optimization (PSO) algorithm in [31]–[33].

V. RECONSTRUCTION

A. RECOVERY ALGORITHM

Now we show how to reconstruct the input signal $x(t)$ from the obtained samples $y[n]$ in (12) and $x[n']$ in (16). The reconstruction scheme is based on the optimization object function proposed in (20). In the reconstruction process as illustrated in Figure 4, the best number of Lorentzian pulses K_{best} is found by testing all possible values. While the best Lorentzian pulse parameters $\mathbf{P}_{best} = \{c_k, d_k, r_k, t_k\}_{k=1}^{K_{best}}$ are estimated by using the improved PSO algorithm proposed in Algorithm 1. Such process can be described as follows:

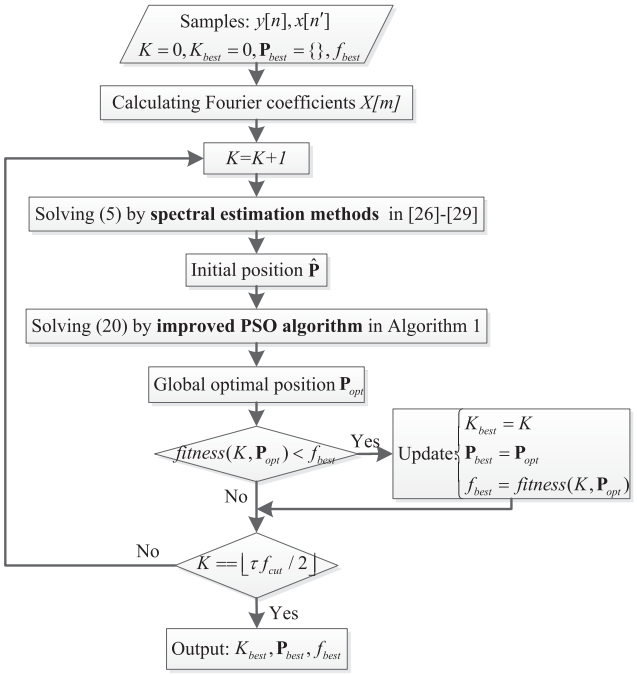

FIGURE 4. Flow chart of the reconstruction process.

Step 1, Initialization. At the beginning, the samples $y[n]$ in (12) and $x[n']$ in (16) are obtained from the proposed sampling system in Figure 3. The number of Lorentzian pulses is set to $K = 0$, the best number of Lorentzian pulses is set to $K_{best} = 0$, the best Lorentzian pulse parameters are set to $\mathbf{P}_{best} = \{\}$ and the best value of (21) is set to f_{best}.

Step 2, Calculating the Fourier coefficients $X[m]$ ($m = 0, 1, \cdots, \lfloor \tau f_{cut} \rfloor$) through (13), (14) and (15), by using the samples $y[n]$.

Step 3, Update the number of Lorentzian pulses $K = K + 1$.

Step 4, Solving (5) with the Fourier coefficients $X[m]$, by using the spectral estimation methods in [26]–[29]. The estimated parameters $\hat{\mathbf{P}} = \{\hat{c}_k, \hat{d}_k, \hat{r}_k, \hat{t}_k\}_{k=1}^{K}$ are used as the initial position of a few selected particles of the improved PSO algorithm proposed in Algorithm 1.

Step 5, Solving the optimization problem of (20) by using the improved PSO algorithm proposed in Algorithm 1. Assume that the global optimal position is $\mathbf{P}_{opt}$.

Step 6, Update the best solutions. If $fitness(K, \mathbf{P}_{opt}) < f_{best}$, then

$$\begin{cases} K_{best} = K \\ \mathbf{P}_{best} = \mathbf{P}_{opt} \\ f_{best} = fitness(K, \mathbf{P}_{opt}) \end{cases} \tag{26}$$

Step 7, Output the results. If $K = \lfloor \tau f_{cut}/2 \rfloor$, the best solutions are output. Otherwise, go back to **Step 3** and repeat.

After the best number of Lorentzian pulses K_{best} and the corresponding parameters $\mathbf{P}_{best} = \{c_k, d_k, r_k, t_k\}_{k=1}^{K_{best}}$ are found, the input signal can be reconstructed as:

$$x_{best}(t) = \sum_{k=1}^{K_{best}} \frac{c_k r_k + d_k(t - t_k)}{\pi \left(r_k^2 + (t - t_k)^2\right)}, \quad 0 \leq t < \tau, \tag{27}$$

where τ is the time duration of the input signal $x(t)$.

To reduce the computational complexity and to improve the convergence rate, we propose an improved PSO algorithm as shown in Algorithm 1, where *rand*() is the random function in the range [0, 1]. In this algorithm. we select a few particles and set the initial position of these particles as the estimated results of the spectral estimation methods in [26]–[29]. For these selected particles, as suggested in [34], only some of the elements of the position (i.e., the parameters of the Lorentzian pulses with negative width) should be updated. This is achieved by setting the velocity of the other elements of the position (i.e., the parameters of the Lorentzian pulses with nonnegative width) to zero. While for other particles, the updating process was carried out for all elements of the position. Assume that the index set of the Lorentzian pulses with negative width is $\Psi \subset \{1, 2, \cdots, K\}$. As shown in Figure 5, for each selected particle, in each searching process, only the misestimated parameters $\{c_k, d_k, r_k, t_k\}_{k\in\Psi}$ are updated. While the right estimated parameters $\{c_k, d_k, r_k, t_k\}_{k\in\Phi}$, where $\Phi = \{1, 2, \cdots, K\} - \Psi$ is the index set of the estimated Lorentzian pulses with nonnegative width, remain unchanged.

B. PRACTICAL CONSIDERATIONS OF REAL ECG SIGNALS

Now we discuss the practical considerations which should be paid attention to when applying our sampling scheme to

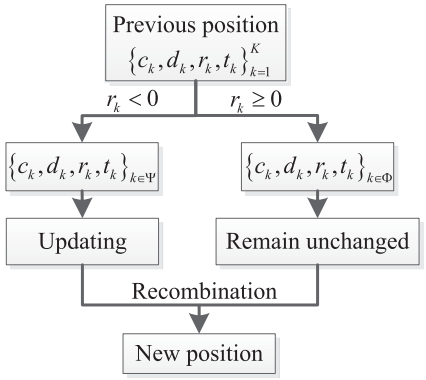

FIGURE 5. Updating process of the position for each selected particle.

real ECG signals. To prevent lifestyle diseases, portable heart beat detection systems by ECG for daily life monitoring have attracted attention [35]. For portable systems, power consumption is critical. It is quite intuitive that a higher sampling rate requires more power when converting a continuous-time signal to digital, since a faster and more precise clock is needed. It is thus beneficial to reduce the sampling frequency at the point of acquisition. Furthermore, a low-sampling rate is also beneficial in reducing the amounts of ECG data for storage and transmission. This will results in a longer duration recording for the patient's ECG, which is desirable for doctors to detect the human body's abnormalities [36]. Thus, sub-Nyquist sampling of ECG signals has advantage in the medical field, especially for portable heart beat detection systems.

First, the medical literatures [37] have declared that there are five different waves in each ECG signal, which can be labeled as P wave, Q wave, R wave, S wave and T wave. Each wave represents a single human heart beat stage. As shown in Figure 6, the P wave and T wave are clear and wide, while the Q wave, R wave and S wave are close and narrow. In practice, the ECG signals exhibit a cyclic behavior due to the repeated human heart beat. At the beginning of each heart beat, the electrical signal polarizes the left and right atria and generates the P wave. After that, the depolarization process results in the QRS complex wave, which is consist of the Q wave, the R wave and the S wave. The duration of these waves are very short while the peaks are large. After a short rest, the repolarization process also behaves as a positive T wave. At the end of the T wave, a new heart beat cycle starts. Therefore, the ECG signals can be split into separate heart beat by segmenting between the P wave and T wave. So we process each heart beat of the ECG signals independently, as [37] declares.

Second, to decrease the effect of noise and improve the recovering performance, we use several denoising techniques borrowed from spectral estimation theory [26]–[29] when initial estimate the unknown parameters. For example, the iterative Cadzow denoising algorithm [38] may be applied to the obtained Fourier coefficients $X[m]$ before being processed with the annihilating filter method. Applying Cadzow iterations tends to reduce the error of the measurements. After denoising, the denoised data matrix can then be used in conjunction with the annihilating filter method. Another widely used denoising techniques are the MUSIC [27] and ESPRIT [28], which are subspace methods. Such techniques are realized by separating the measurement space into signal and noise subspaces. Unlike Cadzow, they are a non-iterative algorithms.

Algorithm 1 Improved PSO Algorithm

Require: Number of particles Num; Learning factors c_1, c_2; Inertia weight w; Number of iterations tf; Number of Lorentzian pulses K; Initial position $\hat{\mathbf{P}}$; Maximum and minimum values of the position $\mathbf{P}_{max}$, $\mathbf{P}_{min}$; Maximum and minimum velocity $\mathbf{V}_{max}$, $\mathbf{V}_{min}$; Number of selected particles S.

Ensure: Global optimal position $\mathbf{P}_{opt}$.

for $i = 1$ to Num **do**
  $\mathbf{V}^i$ is randomly selected in $[\mathbf{V}_{min}, \mathbf{V}_{max}]$;
  if $i \leq S$ **then**
    $\mathbf{P}^i = \hat{\mathbf{P}}$;
  else
    $\mathbf{P}^i$ is randomly selected in $[\mathbf{P}_{min}, \mathbf{P}_{max}]$;
  end if
  $\mathbf{P}^i_{local} = \mathbf{P}^i$;
  $f^i_{local} = fitness(K, \mathbf{P}^i_{local})$;
  if $f^i_{local} < f_{opt}$ **then**
    $\mathbf{P}_{opt} = \mathbf{P}^i_{local}$;
    $f_{opt} = f^i_{local}$;
  end if
end for
for $t = 1$ to tf **do**
  for $i = 1$ to Num **do**
    $\mathbf{V}^i = w * \mathbf{V}^i + c_1 * rand() * (\mathbf{P}^i_{local} - \mathbf{P}^i) + c_2 * rand() * (\mathbf{P}_{opt} - \mathbf{P}^i)$;
    if $i \leq S$ **then**
      for $k = 1$ to K **do**
        if $r_k \geq 0$ **then**
          $\mathbf{V}^i(4k-3:4k) = [0, 0, 0, 0]$;
        end if
      end for
    end if
    $\mathbf{P}^i = \mathbf{P}^i + \mathbf{V}^i$;
    if $fitness(K, \mathbf{P}^i) < f^i_{local}$ **then**
      $\mathbf{P}^i_{local} = \mathbf{P}^i$;
      $f^i_{local} = fitness(K, \mathbf{P}^i_{local})$;
    end if
    if $f^i_{local} < f_{opt}$ **then**
      $\mathbf{P}_{opt} = \mathbf{P}^i_{local}$;
      $f_{opt} = f^i_{local}$;
    end if
  end for
end for

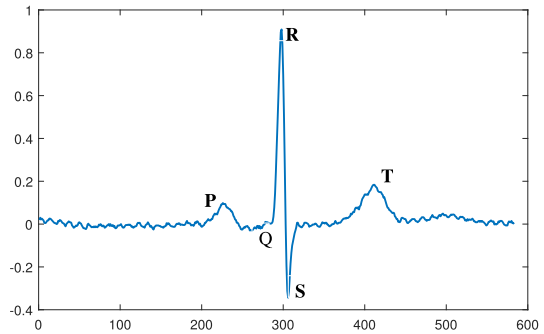

FIGURE 6. Compositions of a real ECG signal.

VI. EXPERIMENTS RESULTS

In this section, we propose several experiments to exam the effectiveness of our method. The ECG signals from the MIT-BIH Arrhythmia Database (mitdb) [39] are used in the experiments. These measurements are originally sampled at the rate 360 Hz. Since the heart beat rate of a human varies from 60 to 80 times per minute, the periodic of each heart beat is about $\tau = 0.75 \sim 1$ sec. In our system as illustrated in Figure 3, the cutoff frequency of LPF is $f_{cut} = 40$ Hz and the sampling rate of the first channel is $f_s = 2f_{cut} = 80$ Hz, which is far below the original sampling rate 360 Hz. For convenience, the sampling rate of the other channel is set to be $f_s' = 80$ Hz too. Then an optimal number of Lorentzian pulses K, where $1 \le K \le \lfloor \tau f_{cut}/2 \rfloor = 15$, can be found by using the proposed reconstruction algorithm.

In the reconstruction process, the parameters of the improved PSO algorithm in Algorithm 1 are listed as follows: Number of particles $Num = 100$; Learning factors $c_1 = c_2 = 1.4962$; Inertia weight $w = 0.7298$; Number of iterations $tf = 200$; Minimum values of the position $\mathbf{P}_{min} = \{-10, -10, -1, 0\}$; Maximum values of the position $\mathbf{P}_{max} = \{10, 10, 1, 2\}$; Minimum velocity $\mathbf{V}_{min} = \{-20, -20, -2, -2\}$; Maximum velocity $\mathbf{V}_{max} = \{20, 20, 2, 2\}$; Number of selected particles $S = 20$. The initial position $\hat{\mathbf{P}}$ is the estimated result of the spectral estimation methods in [26]–[29].

The objective of the experiments can be divided into five parts:

1) Examination of the effectiveness of our method in optimizing the number of Lorentzian pulses K and other pulse parameters;
2) Verification of our method for different shapes of ECG signals;
3) Evaluation of the performance of our method under different sampling rate;
4) Analysis of the effect of model mismatch error for reconstruction of real ECG signals;
5) Comparison of our method and other techniques in the presence of noise.

To conduct quantitative analysis for simulation results, the signal to residual ratio (SRR) in [23] is considered as the evaluation index, which is defined as

$$SRR = 20 \log \left(\frac{\sum_{n=0}^{N-1} x^2[n]}{\sum_{n=0}^{N-1} (x[n] - \hat{x}[n])^2} \right), \tag{28}$$

where $\hat{x}[n]$ is the discrete reconstructed signal. Note that a larger SRR of the reconstruction results represents a smaller squared error.

Simulation 1: The aim of the first experiment is to exam the effectiveness of the proposed method. In the traditional VPW-FRI scheme, it requires that the number of Lorentzian

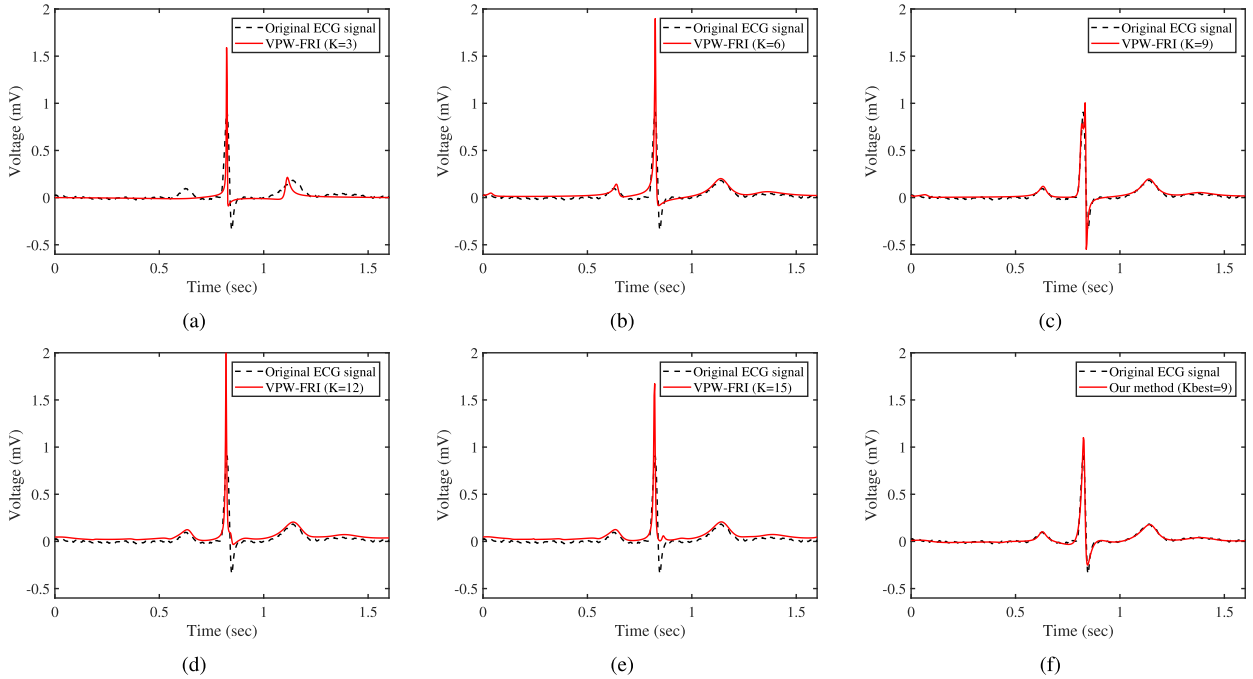

FIGURE 7. Recovery results of a single heart beat: (a) VPW-FRI with K set to be 3; (b) VPW-FRI with K set to be 6; (c) VPW-FRI with K set to be 9; (d) VPW-FRI with K set to be 12; (e) VPW-FRI with K set to be 15; (f) Our method with optimal $K_{best} = 9$.

pulses K is chosen with experience. As is suggested in [23], about $5 \sim 8$ Lorentzian pulses are suitable for modeling one heart beat of ECG signals. So we choose to set $K = 3, 6, 9, 12$. Figure 7 represents an extract recovery of a heart beat of the ECG signal from the database. From Figure 7(a) to Figure 7(e) we can see that the recovery results of VPW-FRI are various with the setting of K. So the VPW-FRI scheme is unstable for ECG signals. Figure 7(f) shows the recovery result of our method, with the optimal number of Lorentzian pulses $K_{best} = 9$. Visually, we clearly see the advantage of optimization process of our method in finding the optimal number of Lorentzian pulses K.

For convenient comparison, we summarize the results of this experiment in Table 1. We introduce the error rate to analyze the stability of the methods, which is defined as

$$ER = \frac{K_{wrong}}{K} \tag{29}$$

where K_{wrong} is the number of wrong pulses, i.e., the estimated Lorentzian pulses with negative width. First, we observe that there may exist several misestimated pulses of VPW-FRI method, which derive from the model mismatch error. These misestimated pulses will be corrected in each searching process of our method. We also observe that the error rate of VPW-FRI is the highest (26.67%) when the number of Lorentzian pulses K is set to be 15, meaning that a higher K does not lead to improve the reconstruction performance. Then, it can be seen that VPW-FRI method achieves the best SRR of 14.94 dB when the value of K is 9. While in our method, we correct the two misestimated pulses with PSO algorithm and improve SRR from 14.94 dB to 26.53 dB, which verify the effectiveness of our method. The comparison of the parameters of VPW-FRI and our method is shown in Table 2. It can be seen from Table 2 that the misestimated pulses of VPW-FRI are pulse 2 ($r_k = -0.0248$) and pulse 7 ($r_k = -0.0160$). In our method, these two pulses have been corrected. In practice, all parameters of pulse 2 $\{c_2, d_2, r_2, t_2\}$ have been improved from $\{1.5902e-06, -4.0102e-06, -0.0248, 0.4105\}$ to $\{-0.0666, -0.0656, 0.4016, 1.0814\}$, and all parameters of pulse 7 $\{c_7, d_7, r_7, t_7\}$ have been improved from $\{2.4196e-05, -5.9343e-07, -0.0160, 1.1744\}$ to $\{0.0455, 0.0850, 0.4050, 0.9987\}$.

Simulation 2: To further verify our method, two more ECG shapes, i.e., ECG record 101 and ECG record 209 from MIT-BIH Arrhythmia Database, have been tested. As shown in Figure 8 and Figure 9, the simulation results demonstrate the effectiveness of the our method. Moreover, we clearly see that the ECG signals reconstructed by our method (red curves) outperform the results reconstructed by VPW-FRI scheme (blue curves).

Simulation 3: Then we study the influence of the sampling rate to our method. According to (23), the sampling rate of the first channel should satisfy $f_s \geq 4K/\tau$. For traditional VPW-FRI scheme, we set the number of Lorentzian pulses

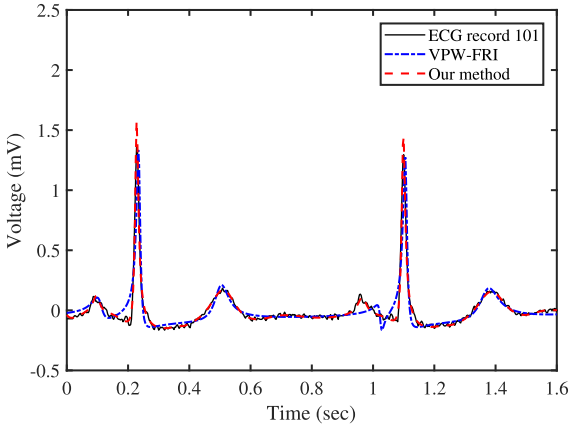

FIGURE 8. Recovery results of ECG record 101 from MIT-BIH Arrhythmia Database.

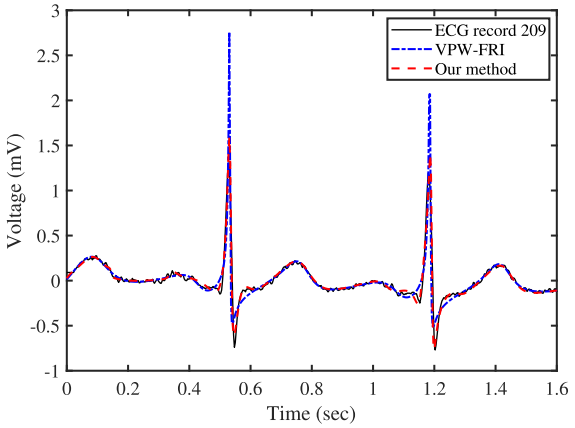

FIGURE 9. Recovery results of ECG record 209 from MIT-BIH Arrhythmia Database.

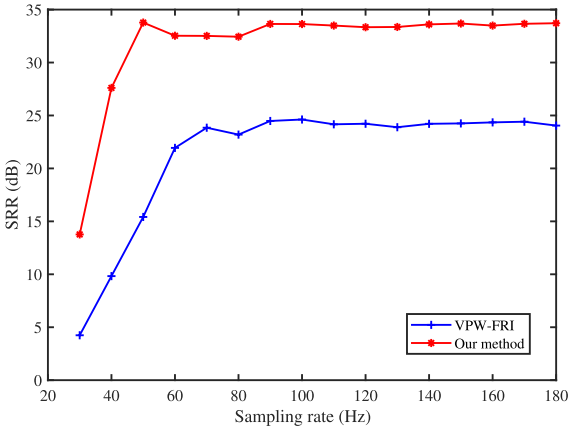

FIGURE 10. Average SRR of real ECG signals under different sampling rate.

$K = 7$, meaning that the lowest sampling rate is 28 Hz. In this simulation, we test our method with 48 ECG signals from the MIT-BIH arrhythmia database with the sampling rate increasing from 30 Hz to 180 Hz. The average results are illustrated in Figure 10. The two curves obviously rise with the sampling rate increasing from 30 Hz to 60Hz, meaning that more Fourier coefficients helps to improve the reconstruction precision. However, we also observe that there is tiny change from around 60 Hz to 180 Hz, meaning that the sampling rate has no influence on the reconstruction

TABLE 1. Comparison of stability and reconstruction quality.

Method	Number of wrong pulses	Error rate (%)	SRR (dB)
VPW-FRI ($K = 3$)	0	0	3.86
VPW-FRI ($K = 6$)	1	16.67	8.54
VPW-FRI ($K = 9$)	2	22.22	14.94
VPW-FRI ($K = 12$)	2	16.67	4.19
VPW-FRI ($K = 15$)	4	26.67	6.58
Our method ($K_{best} = 9$)	0	0	26.53

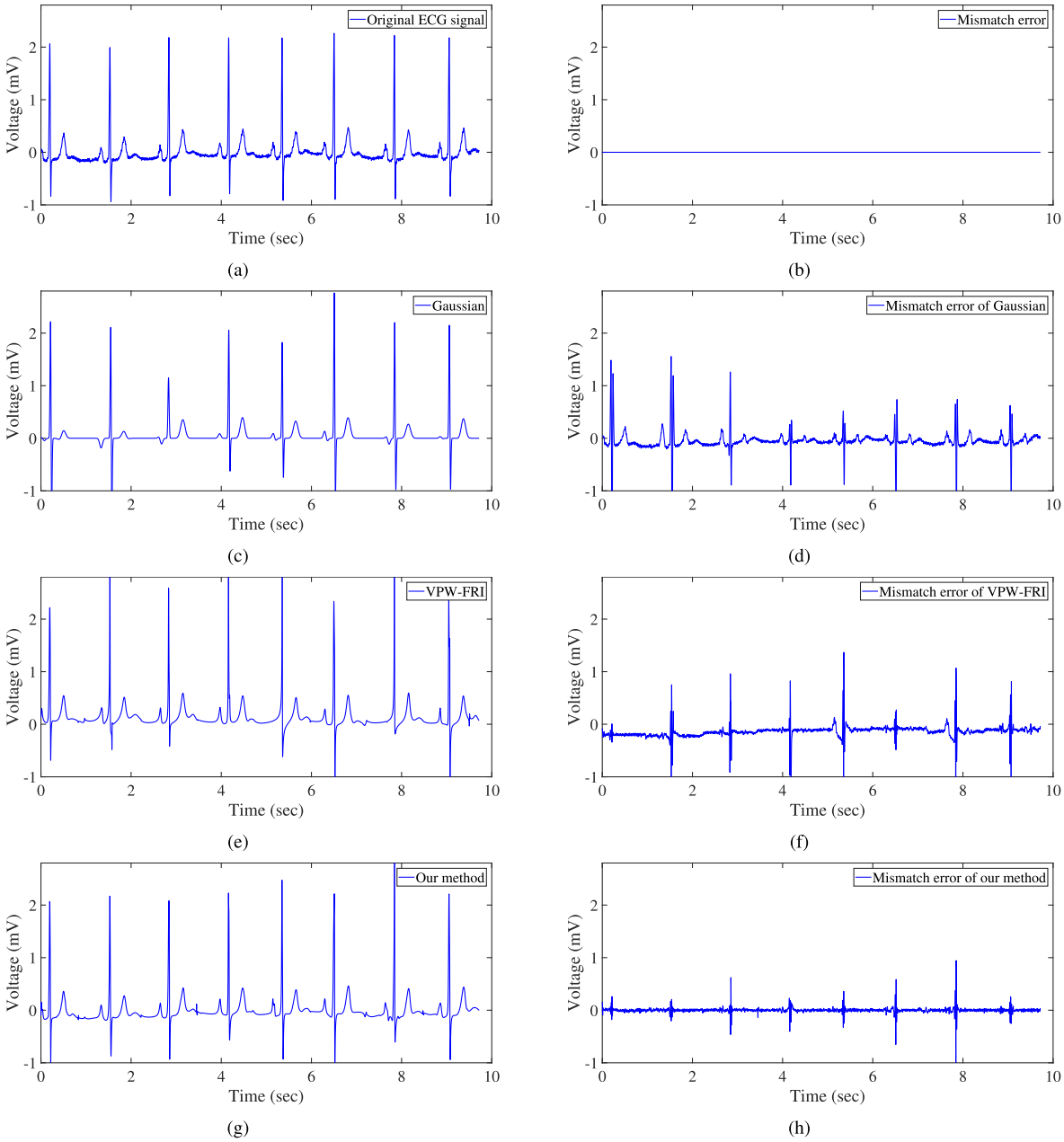

FIGURE 11. Recovery results of ECG record 123: (a) original ECG signal; (b) Model mismatch error signal of original ECG; (c) VPW-FRI estimation with $K = 7$ pulses for each heart beat; (d) Model mismatch error signal of VPW-FRI; (e) Estimation with Gaussian based FRI method; (f) Model mismatch error signal of Gaussian; (g) Estimation with our method; (h) Model mismatch error signal of our method.

performance when the number of Fourier coefficients is large enough. The results also showed that our method outperforms the VPW-FRI method at the same sampling rate.

Simulation 4: The next experiment aims to analyze the model mismatch error of our method in real ECG signals, and compare to the VPW-FRI model in [23]–[25] and the

TABLE 2. Comparison of the parameters of VPW-FRI and our method.

Pulse	VPW-FRI ($K = 9$)				Our method ($K_{best} = 9$)			
(k)	c_k	d_k	r_k	t_k	c_k	d_k	r_k	t_k
1	0.0003	-0.0009	0.0132	0.1019	0.0003	-0.0009	0.0132	0.1019
2	**1.5902e-06**	**-4.0102e-06**	**-0.0248**	**0.4105**	**-0.0666**	**-0.0656**	**0.4016**	**1.0814**
3	0.0086	-0.0031	0.0237	0.6374	0.0086	-0.0031	0.0237	0.6374
4	0.0243	0.0085	0.0097	0.8179	0.0243	0.0085	0.0097	0.8179
5	-0.0060	-0.0071	0.0019	0.8426	-0.0060	-0.0071	0.0019	0.8426
6	0.0283	0.0043	0.0461	1.1286	0.0283	0.0043	0.0461	1.1286
7	**2.4196e-05**	**-5.9343e-07**	**-0.0160**	**1.1744**	**0.0455**	**0.0850**	**0.4050**	**0.9987**
8	0.0090	0.0054	0.0739	1.3704	0.0090	0.0054	0.0739	1.3704
9	-0.0001	0.0002	0.0028	1.5888	-0.0001	0.0002	0.0028	1.5888

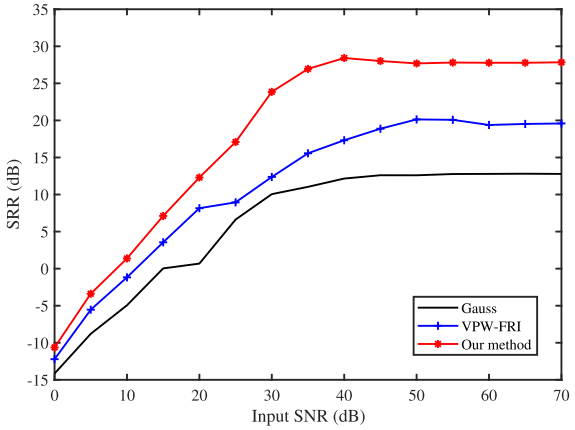

FIGURE 12. Comparison of different approaches in the presence of noise.

Gaussian model described in [22]. Since these methods are all based on Fourier coefficients of the input signal, we use the same sampling structure as the first channel of our system. That is, a LPF with cutoff frequency $f_{cut} = 40$ Hz, followed by sampling at the rate $f_s = 2f_{cut} = 80$ Hz. So about 41 Fourier coefficients can be obtained. Figure 11 shows the experimental results of the ECG record 123 in MIT-BIH database. Obviously, for original ECG signal, the model mismatch error is 0. We can observe that the Gaussian method has no ability to recover the low amplitude pulses of the ECG signal. The model mismatch error signal of our method is much better than the traditional VPW-FRI method, mainly due to the optimization process in the reconstruction.

Simulation 5: Finally, we compare our method with the other Fourier spectrum based methods in the presence of noise. For the VPW-FRI method in [23]–[25] and the Gaussian method in [22], the setup of the acquisitions is the same as in Simulation 3. In this simulation, we test our method with 48 ECG signals from the MIT-BIH arrhythmia database with the signal-to-noise ratio (SNR) of the additive white Gaussian noise increasing from 0 dB to 70 dB. The experimental tests were carried out 100 times. The average SRR has been measured and compared with the input SNR of the noise. Simulation results are shown in Figure 12. We see that our method outperforms the VPW-FRI method and Gaussian method about 2-3 dB at the input SNR of 0-15 dB. This is because the frequency aperture plays a dominant role when SNR is very low. Since the Fourier coefficients are the same for all these methods, the diversity of reconstruction is not significant at low input SNR. As the SNR increasing, the model mismatch error plays more significant role. We see that our method outperforms the VPW-FRI method and Gaussian method much more at the input SNR from 15 dB to 35 dB. Such results are due to the fact that our method provides an efficient way to minimize the energy of the model mismatch error signal. For high enough SNR values (i.e., 35 dB), the reconstruction results tend to be stable.

VII. CONCLUSIONS

In this paper, we propose an optimization model based sub-Nyquist sampling system for pulses with various shapes to improve the performance of the VPW-FRI scheme under noise and model mismatch situations. The proposed system consists of two sub-Nyquist sampling channels, with a LPF and two low rate ADCs in total. To reduce the effort of noise and model mismatch, we build an optimization function and solve it with the obtained frequency and time domain samples, by using the PSO algorithm. We demonstrate that the optimal number of Lorentzian pulses and the corresponding pulse parameters can be found by our method. According to the simulations with real ECG records from the MIT-BIH arrhythmia database, our method achieves better performance and stability than previous technologies, even under noise situations.

REFERENCES

[1] L. Zhou, G. Han, and L. Liu, "Pulse-based distance accumulation localization algorithm for wireless nanosensor networks," *IEEE Access*, vol. 5, pp. 14380–14390, 2017.
[2] D. Yang, J. Hu, and S. Liu, "A low profile UWB antenna for WBAN applications," *IEEE Access*, vol. 6, pp. 25214–25219, 2018.
[3] Y. Sun, L. Zheng, P. Zhu, and X. Wang, "On optimality of local maximum-likelihood detectors in large-scale MIMO channels," *IEEE Trans. Wireless Commun.*, vol. 15, no. 10, pp. 7074–7088, Oct. 2016.
[4] H.-S. Choi, B. Lee, and S. Yoon, "Biometric authentication using noisy electrocardiograms acquired by mobile sensors," *IEEE Access*, vol. 4, pp. 1266–1273, 2016.
[5] M. Elgendi, A. Al-Ali, A. Mohamed, and R. Ward, "Improving remote health monitoring: A low-complexity ECG compression approach," *Diagnostics*, vol. 8, no. 1, p. 10, 2018. [Online]. Available: http://www.mdpi.com/2075-4418/8/1/10

[6] J. Park, J. Jang, S. Im, and H.-N. Lee, "A sub-Nyquist radar electronic surveillance system," *IEEE Access*, vol. 6, pp. 10080–10091, 2018.
[7] L. Zheng and X. Wang, "Super-resolution delay-Doppler estimation for OFDM passive radar," *IEEE Trans. Signal Process.*, vol. 65, no. 9, pp. 2197–2210, May 2017.
[8] X. Liang, H. Zhang, G. Fang, S. Ye, and T. A. Gulliver, "An improved algorithm for through-wall target detection using ultra-wideband impulse radar," *IEEE Access*, vol. 5, pp. 22101–22118, 2017.
[9] M. Unser, "Sampling-50 years after Shannon," *Proc. IEEE*, vol. 88, no. 4, pp. 569–587, Apr. 2000.
[10] M. Vetterli, P. Marziliano, and T. Blu, "Sampling signals with finite rate of innovation," *IEEE Trans. Signal Process.*, vol. 50, no. 6, pp. 1417–1428, Jun. 2002.
[11] I. Maravic and M. Vetterli, "Sampling and reconstruction of signals with finite rate of innovation in the presence of noise," *IEEE Trans. Signal Process.*, vol. 53, no. 8, pp. 2788–2805, Aug. 2005.
[12] T. Blu, P.-L. Dragotti, M. Vetterli, P. Marziliano, and L. Coulot, "Sparse sampling of signal innovations," *IEEE Signal Process. Mag.*, vol. 25, no. 2, pp. 31–40, Mar. 2008.
[13] P. L. Dragotti, M. Vetterli, and T. Blu, "Sampling moments and reconstructing signals of finite rate of innovation: Shannon meets Strang–Fix," *IEEE Trans. Signal Process.*, vol. 55, no. 5, pp. 1741–1757, May 2007.
[14] R. Tur, Y. C. Eldar, and Z. Friedman, "Innovation rate sampling of pulse streams with application to ultrasound imaging," *IEEE Trans. Signal Process.*, vol. 59, no. 4, pp. 1827–1842, Apr. 2011.
[15] K. Gedalyahu, R. Tur, and Y. C. Eldar, "Multichannel sampling of pulse streams at the rate of innovation," *IEEE Trans. Signal Process.*, vol. 59, no. 4, pp. 1491–1504, Apr. 2011.
[16] E. Baransky, G. Itzhak, N. Wagner, I. Shmuel, E. Shoshan, and Y. Eldar, "Sub-Nyquist radar prototype: Hardware and algorithm," *IEEE Trans. Aerosp. Electron. Syst.*, vol. 50, no. 2, pp. 809–822, Apr. 2014.
[17] G. Huang, N. Fu, L. Qiao, J. Cao, and C. Fan, "A simplified FRI sampling system for pulse streams based on constraint random modulation," *IEEE Trans. Circuits Syst. II, Exp. Briefs*, vol. 65, no. 2, pp. 256–260, Jun. 2018.
[18] N. Fu, G. Huang, L. Qiao, and H. Zhao, "Sub-Nyquist sampling and recovery of pulse streams with the real parts of Fourier coefficients," *IEEE Access*, vol. 5, pp. 22667–22677, 2017.
[19] I. Maravic, J. Kusuma, and M. Vetterli, "Low-sampling rate UWB channel characterization and synchronization," *J. Commun. Netw.*, vol. 5, no. 4, pp. 319–327, Dec. 2003.
[20] Y. Zhang and P. L. Dragotti, "On the reconstruction of wavelet-sparse signals from partial Fourier information," *IEEE Signal Process. Lett.*, vol. 22, no. 9, pp. 1234–1238, Sep. 2015.
[21] Y. Zhang and P. L. Dragotti, "Sampling streams of pulses with unknown shapes," *IEEE Trans. Signal Process.*, vol. 64, no. 20, pp. 5450–5465, Oct. 2016.
[22] S. Nagesh and C. S. Seelamantula, "FRI sampling and reconstruction of asymmetric pulses," in *Proc. IEEE Int. Conf. Acoust., Speech Signal Process. (ICASSP)*, Apr. 2015, pp. 5957–5961.
[23] G. Baechler, A. Scholefield, L. Baboulaz, and M. Vetterli, "Sampling and exact reconstruction of pulses with variable width," *IEEE Trans. Signal Process.*, vol. 65, no. 10, pp. 2629–2644, May 2017.
[24] G. Baechler, N. Freris, R. F. Quick, and R. E. Crochiere, "Finite rate of innovation based modeling and compression of ECG signals," in *Proc. IEEE Int. Conf. Acoust., Speech Signal Process.*, May 2013, pp. 1252–1256.
[25] A. Nair and P. Marziliano, "Fetal heart rate detection using VPW-FRI," in *Proc. IEEE Int. Conf. Acoust., Speech Signal Process. (ICASSP)*, May 2014, pp. 4438–4442.
[26] T. K. Sarkar and O. Pereira, "Using the matrix pencil method to estimate the parameters of a sum of complex exponentials," *IEEE Antennas Propag. Mag.*, vol. 37, no. 1, pp. 48–55, Feb. 1995.
[27] R. O. Schmidt, "Multiple emitter location and signal parameter estimation," *IEEE Trans. Antennas Propag.*, vol. AP-34, no. 3, pp. 276–280, Mar. 1986.
[28] R. Roy, A. Paulraj, and T. Kailath, "ESPRIT—A subspace rotation approach to estimation of parameters of cisoids in noise," *IEEE Trans. Acoust. Speech, Signal Process.*, vol. 34, no. 5, pp. 1340–1342, Oct. 1986.
[29] Y. C. Eldar, *Sampling Theory: Beyond Bandlimited Systems*. Cambridge, U.K.: Cambridge Univ. Press, 2015.
[30] N. Fu, G. Huang, L. Zheng, and X. Wang, "Sub-Nyquist sampling of multiple sinusoids," *IEEE Signal Process. Lett.*, vol. 25, no. 4, pp. 581–585, Apr. 2018.
[31] G. Abbas, J. Gu, U. Farooq, A. Raza, M. U. Asad, and M. E. El-Hawary, "Solution of an economic dispatch problem through particle swarm optimization: A detailed survey—Part II," *IEEE Access*, vol. 5, pp. 24426–24445, 2017.
[32] X. Zhang, K. Song, C. Li, and L. Yang, "Parameter estimation for multi-scale multi-lag underwater acoustic channels based on modified particle swarm optimization algorithm," *IEEE Access*, vol. 5, pp. 4808–4820, 2017.
[33] M. H. Ali, B. A. D. Al Mohammed, A. Ismail, and M. F. Zolkipli, "A new intrusion detection system based on fast learning network and particle swarm optimization," *IEEE Access*, vol. 6, pp. 20255–20261, 2018.
[34] G. Baechler, "Sensing ECG signals with variable pulse width finite rate of innovation," M.S. thesis, École Polytechn. Fédérale de Lausanne, Lausanne, Switzerland, 2012.
[35] A. Temko, "Accurate heart rate monitoring during physical exercises using PPG," *IEEE Trans. Biomed. Eng.*, vol. 64, no. 9, pp. 2016–2024, Sep. 2017.
[36] Y.-H. Tseng, Y.-H. Chen, and C.-W. Lu, "Adaptive integration of the compressed algorithm of CS and NPC for the ECG signal compressed algorithm in VLSI implementation," *Sensors*, vol. 17, no. 10, p. 2288, 2017. [Online]. Available: http://www.mdpi.com/1424-8220/17/10/2288
[37] L. Sörnmo and P. Laguna, *Bioelectrical Signal Processing in Cardiac and Neurological Applications* . New York, NY, USA: Academic, 2005.
[38] J. A. Cadzow, "Signal enhancement—A composite property mapping algorithm," *IEEE Trans. Acoust., Speech, Signal Process.*, vol. ASSP-36, no. 1, pp. 49–62, Jan. 1988.
[39] A. L. Goldberger *et al.*, "PhysioBank, PhysioToolkit, and PhysioNet: Components of a new research resource for complex physiologic signals," *Circulation*, vol. 101, no. 23, pp. E215–E220, 2000.

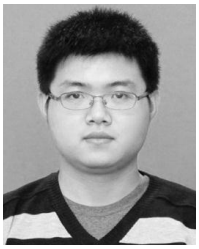

GUOXING HUANG received the B.S. degree from the University of Science and Technology Beijing, China, in 2010, and the M.S. degree from Liaoning University, China, in 2013.

He is currently pursuing the Ph.D. degree with Automatic Test and Control Department, Harbin Institute of Technology. His main research interests include sampling with finite rate of innovation, compressive sensing, and signal processing.

NING FU received the B.S., M.S., and Ph.D. degrees from the Harbin Institute of Technology (HIT), Harbin, China, in 2002, 2004, and 2009, respectively.

Since 2012, he has been an Associate Professor with Automatic Test and Control Department, HIT. He has published over 30 journal and conference papers. His current research interests include information acquisition theory, compressive sensing, and automatic test technology.

LIYAN QIAO received the B.S., M.S., and Ph.D. degrees from the Harbin Institute of Technology (HIT), Harbin, China, in 1996, 1998, and 2005, respectively.

Since 2009, he has been a Professor with Automatic Test and Control Department, HIT. He has published over 40 journal and conference papers. His current research interests include data acquisition technology, mass-storage data record technology, and test information processing.